Extended Finite Element Method for Fretting Fatigue Crack Propagation

E. Giner [a,*], N. Sukumar [b], F.D. Denia [a], F.J. Fuenmayor [a]

[a] *Departamento de Ingeniería Mecánica y de Materiales*

Universidad Politécnica de Valencia, Camino de Vera, 46022 Valencia, Spain.

[b] *Department of Civil and Environmental Engineering*

University of California, One Shields Avenue, Davis, CA 95616, USA.

Abstract

In this paper, the extended finite element method (X-FEM) is considered for the analysis of fretting fatigue problems. A two-dimensional implementation of the X-FEM is carried out within the finite element software ABAQUS^{TM} by means of user subroutines, and crack propagation in fretting fatigue problems is investigated. On utilizing the non-linear contact capabilities of this code, the numerical technique is applied to a specimen-indenter model. The use of the X-FEM facilitates very accurate stress intensity factor computations on relatively coarse meshes, and furthermore, no remeshing is required for crack growth simulations. The implementation is applied to complete and incomplete contact fretting problems. A study of crack growth is conducted for several bulk loads applied to the specimen, and the influence of the initial crack angle is ascertained. The numerical simulations reveal the merits of applying the X-FEM to fretting fatigue problems.

Key words: fretting fatigue; crack propagation; extended finite element method; frictional contact.

* Corresponding author. Tel.: +34-96-3877621; fax: +34-96-3877629.
Email address: eginerm@mcm.upv.es (E. Giner).

1 INTRODUCTION

Problems in fretting fatigue are characterized by the presence of two or more contacting bodies, subjected to relative displacements of small amplitude. Under these conditions, the stresses exhibit steep gradients in the vicinity of the contact zone. The combination of such a high stress gradient with the cyclic nature of the loading leads to the nucleation of small cracks that often propagate until the eventual failure of the component (hence the term fretting fatigue). In practice, two different stages are distinguished during this process: crack nucleation and crack propagation.

In fretting fatigue, nucleation processes are usually relatively fast, due to the strong tractions on the contacting surfaces. Hence, under these circumstances, most of the component life is spent in the propagation stage (Sheikh et al., 1994; Adibnazari and Hoeppner, 1994; Hattori et al., 2003). Thus a fracture mechanics approach is usually considered to be appropriate to estimate fretting fatigue propagation life (Faanes and Fernando, 1994; Faanes, 1995; Hills and Nowell, 1994). In this study, the nucleation or initiation stage is not considered and a fully-formed crack is assumed. Its size will be such that the surrounding material is assumed to be homogeneous and isotropic, i.e. the crack length is greater than several material grains (Hills and Nowell, 1994; Dai et al., 1994).

The propagation stage in a fretting fatigue problem is substantially different from that of plain fatigue during the phase in which the crack length is less than the characteristic dimension of the contact zone (Hills and Nowell, 1994; Dai et al., 1994). In such a situation, it is essential to account for the effect of

the contact stress field on the crack and vice versa (contact-crack interaction). It is especially important to estimate realistic values of the stress intensity factors (SIFs) and as a consequence, numerical modelling often becomes a necessity (for example, using the finite element method, FEM).

Due to the intrinsic complexity of modelling fretting fatigue, simplifications are often introduced. Several authors have studied the propagation stage in two dimensions. Faanes and Härkegård (1994) calculated K_{I} analytically by applying equivalent contact tractions and Green's functions. They assumed either straight cracks growing in a normal direction to the contact surface or inclined cracks (Faanes, 1995). Kimura and Sato (2003) used a similar approach extended to inclined mixed-mode cracks. Sheikh et al. (1994) used a FE model of the classic fretting bridge and studied the SIFs for several crack lengths and different crack angles with respect to the contact surface. Mutoh et al. (2003) presented one of the most comprehensive experimental and numerical studies on crack propagation for a fretting bridge configuration. Their FE model included the contact influence, with the crack located at the end of the contact zone. They considered several crack propagation increments to simulate the crack growth path and applied the estimated values of the SIFs to compute the fretting fatigue life. General strategies for predicting the crack growth path in LEFM can be found in the works of Sumi (1985) and Rubinstein (1991).

As opposed to earlier FE approaches, in recent years the extended finite element method (X-FEM) (Moës et al., 1999) has proven to be a very efficient tool for the numerical modelling of cracks in LEFM. In this study, the method is applied to 2D crack analysis under fretting conditions. In comparison to the standard finite element method, the X-FEM provides significant benefits in

the numerical modelling of crack propagation. The main advantages are that the finite element mesh need not to conform to the crack boundaries (crack faces) to account for the geometric discontinuity, and furthermore, mesh regeneration is not needed in crack growth simulations. Therefore, only a single mesh, which is often easily generated, can be used for any crack length and orientation. The X-FEM is based on the introduction of additional degrees of freedom (dofs), which are associated with the nodes of the elements intersected by the crack geometry. These extra dofs in combination with special functions enable the accurate modelling of the crack.

In this paper, we assume a small initial crack that is located near the contact zone, and crack propagation is studied using the extended finite element method. The objective is to determine the influence of the contact stress field on the crack growth path. We assume that the crack is open at the maximum bulk load on the specimen, and therefore the contact between crack faces is not modelled in this work. Several situations are studied, combining different initial cracks and load combinations. The use of the X-FEM enables the evaluation of the influence of the contact zone on crack propagation in a very efficient way. Moreover, it permits to estimate accurate values of the SIF along the crack path by combining energetic post-processing techniques, like the equivalent domain integral form of the J-integral (EDI method) or the interaction integral. An analogous study using a standard finite element formulation would be far less accurate and prohibitively costly, because of the need for mesh regeneration for each crack length and orientation.

2 FUNDAMENTALS OF THE X-FEM

In a standard finite element formulation, a crack must conform to the finite element mesh and remeshing is required to conduct crack propagation simulations. In contrast, in the X-FEM, a crack is modeled via the displacement approximation—a function that is discontinuous across the crack is added to the displacement approximation to model the presence of a crack. Therefore, crack growth can be done without the need for remeshing. This engenders additional degrees of freedom (dofs) that are tied to the nodes of the elements intersected by the crack. The displacement approximation for crack modelling in the extended finite element method takes the form (Moës et al., 1999):

$$\mathbf{u}^h(\mathbf{x}) = \sum_{i=1}^{n} N_i(\mathbf{x}) \left[\mathbf{u}_i + \underbrace{H(\mathbf{x})\mathbf{a}_i}_{\text{only Heaviside nodes}} + \underbrace{\sum_{\alpha=1}^{4} F_\alpha(\mathbf{x})\mathbf{b}_{i\alpha}}_{\text{only crack-tip nodes}} \right], \tag{1}$$

where n is the number of nodes in the mesh, $N_i(\mathbf{x})$ is the shape function of node i, $\mathbf{u}_i$ is the classical dof of node i, and $\mathbf{a}_i$ and $\mathbf{b}_{i\alpha}$ are the dofs associated with the Heaviside step function $H(\mathbf{x})$ and the crack-tip functions $F_\alpha(\mathbf{x})$, respectively. The discontinuous function $H(\mathbf{x})$ takes on the value $+1$ above the crack and -1 below the crack. The crack-tip functions $F_\alpha(\mathbf{x})$ provide improved accuracy and are required if the crack-tip terminates inside an element. These functions are

$$[F_\alpha(r,\theta),\ \alpha = 1\text{–}4] = \left[\sqrt{r}\sin\frac{\theta}{2},\ \sqrt{r}\cos\frac{\theta}{2}, \sqrt{r}\sin\frac{\theta}{2}\sin\theta, \sqrt{r}\cos\frac{\theta}{2}\sin\theta \right], \tag{2}$$

where r, θ are local polar co-ordinates defined at the crack-tip. Further details on the criteria for the selection of enriched nodes and on the implementation of X-FEM can be found in Moës et al. (1999) and Sukumar and Prévost (2003).

Fig. 1 shows a portion of a mesh. The circled nodes are the nodes enriched with 2 additional dofs (total 4 dofs per node) whereas the nodes marked with a square are enriched by 8 more dofs (total 10 dofs per node). Elements that contain at least one enriched node are known as enriched elements. Nodes with 2 additional dofs (one for each co-ordinate direction) have shape functions that multiply $H(\mathbf{x})$. Nodes with 8 additional dofs are enriched in the two Cartesian directions with $F_\alpha(\mathbf{x})$. To compute the element stiffness matrix, the elements that are intersected by the crack are subdivided into subelements for numerical integration. In this study, we have used 7 integration points in triangular subelements and 5×5 quadrature points in quadrilateral subelements as well as in elements that are not subdivided but contain at least one enriched node.

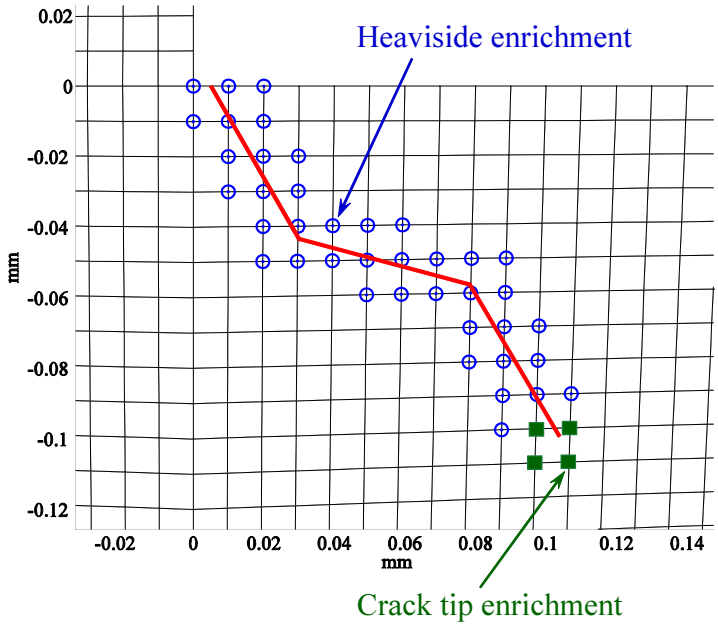

Fig. 1. Enriched nodes in the X-FEM. Circles: nodes with 2 additional dof. Squares: nodes with 8 additional dof.

3 IMPLEMENTATION AND POST-PROCESSING

In this study, we have implemented the X-FEM in the FE commercial code ABAQUS (Hibbitt et al., 2004). To our knowledge, this is one of the first implementations of X-FEM for crack growth simulations within ABAQUS. In the interest of space, just the main features are mentioned. The analysis procedure is as follows. After a single mesh generation, geometric computations based on an exact crack description are carried out to determine the nodes and elements to be enriched, following the approach described in Moës et al. (1999). Next, the ABAQUS solver is called to link the user subroutines that incorporate the X-FEM. The SIFs are then extracted using post-processing techniques and a crack propagation increment is computed. This increment is added to the existing crack geometry and the analysis procedure is repeated.

The ABAQUS user-element capability has been used to formulate the enriched elements. The user-element enables the definition of elements with several dofs per node. ABAQUS capabilities are limited insofar as user-elements can not be directly used as part of contacting surfaces in contact problems nor can user-elements be visualized for plotting purposes. We have overcome these problems using standard 4-node linear elements with very small (negligible) stiffness connected to the nodes of every enriched element and retaining the same connectivity. These *overlay elements* can then be part of the contact pair surfaces to model the contact problem in ABAQUS. Note that the *overlay elements* of negligible stiffness are added in parallel to the user-elements, preserving the actual stiffness of the model. As a consequence, displacements associated with overlay elements are governed by the underlying X-FEM elements. In addition, this enables the representation of a linearly interpolated

deformed shape of the enriched elements.

From Eq. (1), it is clear that the physical displacement at an enriched node i, $\mathbf{u}^h(\mathbf{x}_i)$ is given by the standard dof $\mathbf{u}_i$ plus the enriched contribution $H(\mathbf{x}_i)\mathbf{a}_i$ or $F_\alpha(\mathbf{x}_i)\mathbf{b}_{i\alpha}$. This implies that the standard dof $\mathbf{u}_i$ (the ones used by ABAQUS in its internal contact algorithm or for plotting) do not correspond to the true displacement computed with the X-FEM. In order to make the dof $\mathbf{u}_i$ of an enriched node i be the physical solution of the nodal displacement, the X-FEM has been implemented according to the following modification of Eq. (1), the so-called shifted-basis enrichment (Zi and Belytschko , 2003; Ventura et al., 2003):

$$\mathbf{u}^h(\mathbf{x}) = \sum_{i=1}^{n} N_i(\mathbf{x}) \left[\mathbf{u}_i + \underbrace{\left[H(\mathbf{x}) - H(\mathbf{x}_i)\right]\mathbf{a}_i}_{\text{only Heaviside nodes}} + \underbrace{\sum_{\alpha=1}^{4} \left[F_\alpha(\mathbf{x}) - F_\alpha(\mathbf{x}_i)\right]\mathbf{b}_{i\alpha}}_{\text{only crack-tip nodes}} \right] . \quad (3)$$

The above procedure has proven to be a very good way to combine user-elements with the contact algorithm capabilities available within ABAQUS.

To extract the SIFs, we use the domain form of the interaction integral (Chen and Shield, 1977; Yau et al., 1980). The details on the derivation and its implementation in the X-FEM is available in the literature (Moës et al., 1999; Sukumar and Prévost, 2003; Huang et al., 2003). For the crack orientation prediction based on the values of K_{I} and K_{II}, the MTS criterion proposed by Erdogan and Sih (1963) (maximum tangential stress or hoop stress $\sigma_{\theta\theta}$) is used:

$$\theta_c = \arccos\left(\frac{3K_{\mathrm{II}}^2 + \sqrt{K_{\mathrm{I}}^4 + 8K_{\mathrm{I}}^2 K_{\mathrm{II}}^2}}{K_{\mathrm{I}}^2 + 9K_{\mathrm{II}}^2}\right), \quad (4)$$

where θ_c is the angle that will follow the crack for each of the crack increments. θ_c is measured with respect to a local polar co-ordinate system with its origin

at the crack tip and aligned with the direction of the existing crack. The sign convention is such that $\theta_c < 0$ when $K_{\mathrm{II}} > 0$ and vice versa. Other criteria lead to very similar orientation angles for 2D problems (see a recent review by Richard et al., 2005).

Orientation criteria are well-established for the determination of crack propagation angles under proportional mixed-mode conditions. However, it is reported (Lamacq et al., 1996; Dubourg and Lamacq, 2000) that new criteria or extensions of these criteria are needed under the strong non-proportional conditions of fretting fatigue loading cycles. Under non-proportional conditions, the predicted crack angle is different at each step of the loading cycle. It is claimed that the crack orientation is governed by the direction in which the *amplitude* of the mode I opening during the cycle is maximum (not only the maximum value of the opening). Criteria based on the maximum value of Δk_{I}^* and other modifications seem to yield good estimates under certain conditions (Lamacq et al., 1996; Dubourg and Lamacq, 2000), where k_{I}^* is the mode I SIF associated with an infinitesimal kinked crack emanating from the existing crack in a given direction (see for example Anderson, 1995). For the two problems and loading conditions analyzed in this work (which are described in the next section), we have verified that the criterion based on $\max(\Delta k_{\mathrm{I}}^*)$ over a cycle yields virtually the same results as the MTS criterion applied at the instant of maximum bulk loading, as exemplified in Fig. 2. This figure is computed for a given crack increment of the first problem with a maximum bulk stress of $\sigma_{\mathrm{B,max}} = 60$ MPa. It can be seen that the maximum effective range Δk_{I}^* is attained at the same angle that maximizes k_{I}^* for the maximum bulk loading. Therefore, Eq. (4) has been used at that instant.

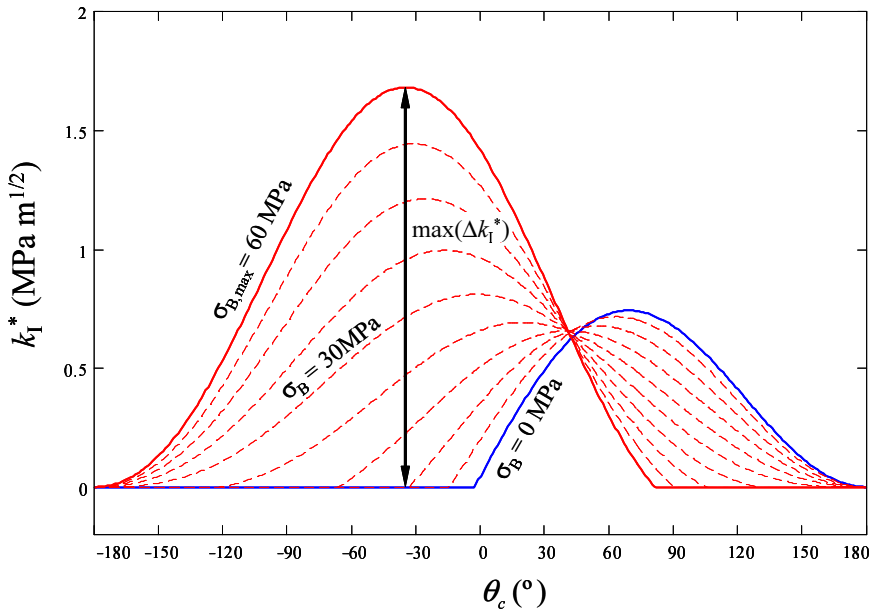

Fig. 2. Mode I SIF associated with an infinitesimal kinked crack emanating from an existing crack. Non-proportional evolution under varying bulk load for Problem 1.

4 NUMERICAL MODELS

Crack propagation in two fretting fatigue test configurations are studied using the extended finite element method. First, a complete contact problem is considered, in which squared-ended indenters are pressed on both sides of a flat specimen. This problem is used here as a benchmark problem to show the merits of the approach for parametric crack growth studies. We have tested the sensitivity of certain parameters to the crack trajectories, such as length and angle of the assumed initial crack or the crack growth increment used in each growing step. In order to verify the accuracy of the X-FEM, we have also compared the SIFs estimations to other solutions obtained by analytical approaches. In addition, a second problem is modelled that represents an incomplete contact with cylindrical indenters. This problem is introduced to demonstrate the robustness of the X-FEM implementation in the presence of

relatively large sliding zones.

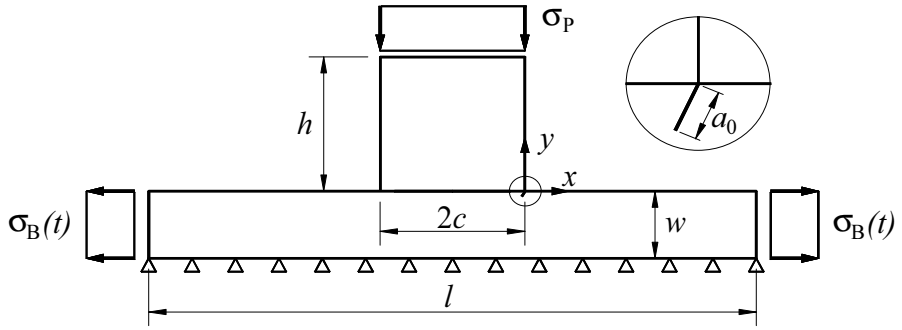

Fig. 3. Problem 1: complete contact model with flat indenters.

The first problem consists of a rectangular specimen subjected to a variable bulk stress and pressed by two opposite square-angled indenters (see Fig. 3). The model dimensions are $h = 2c = 2w = 10$ mm, $l = 40$ mm. The material considered is aluminum alloy 7075-T6, with $E = 72$ GPa and $\nu = 0.3$. Plane strain condition is assumed (although the SIF values are independent of this state) and the friction coefficient is taken as $f = 0.8$ (see Mutoh et al., 2003). The normal load is constant, with a value of $\sigma_{\mathrm{P}} = 60$ MPa and the bulk load is cyclical, with a stress ratio $R = -1$ and a maximum amplitude denoted by $\sigma_{\mathrm{B,max}}$. Five different values of $\sigma_{\mathrm{B,max}}$ have been analyzed (20, 40, 60, 120 and 180 MPa).

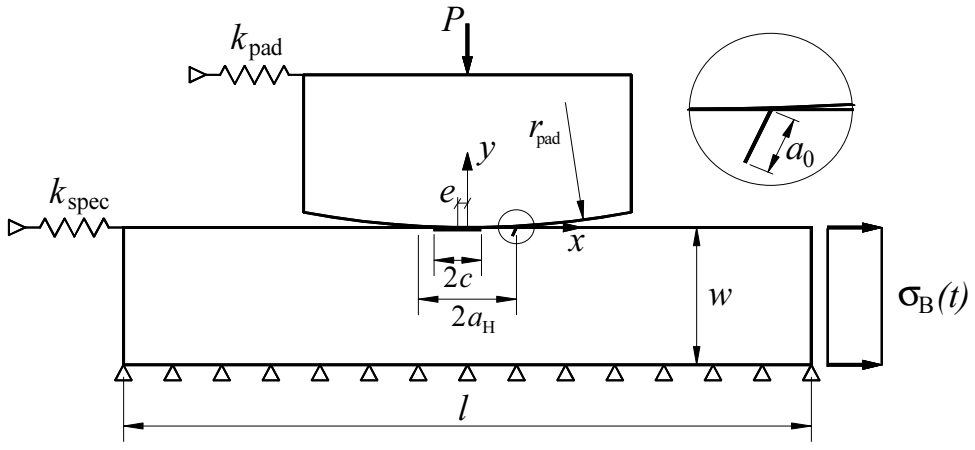

Fig. 4. Problem 2: incomplete contact model with cylindrical pads.

The second problem represents an incomplete contact originated by cylindrical fretting pads of radius $r_{\text{pad}} = 25$ mm. A sketch is shown in Fig. 4, with dimensions $l = 2w = 20$ mm. The normal load $P = 40$ kN is held constant during the test producing a Hertzian contact region of semi-width $a_{\text{H}} = 177.9\ \mu$m, having assumed the same material as in the first problem. A variable bulk stress with a maximum value of $\sigma_{\text{B,max}} = 90$ MPa is applied to the right end of the specimen. Because of the frictional contact and the way the pad is supported, a tangential load Q is generated on the fretting pad. The values of the tangential load and the bulk stress on the left part of the specimen depend on the compliances of both the specimen and the fretting pad support. These compliances are represented in the model by spring elements of stiffnesses k_{spec} and k_{pad}, respectively. We have used multi-point constraints (MPCs) to guarantee an even distribution of point forces over the application side. The specimen spring is attached to a node linked through MPCs to the rest of nodes of the left boundary. They share the same dof in the x-direction. In this way, the force exerted by the spring is equivalent to a distributed load along the whole left side of the specimen. The spring attached to the indenter acts in an analogous manner with respect to the top of the indenter. Under these loading conditions, the contact area of width $2a_{\text{H}}$ has an internal stick zone of width $2c$, located between two slip zones (Hills and Nowell, 1994). The stick zone has an eccentricity e measured from the center of the contact zone (see Fig. 4). The spring stiffnesses k_{spec} and k_{pad} have been calibrated to obtain a tangential load $Q/fP = 0.6$. This corresponds to a sticking zone of size $c/a_{\text{H}} = 0.634$ and eccentricity $e/a_{\text{H}} = 0.210$.

Under reverse cyclic load (i.e. $R = -1$), it is worth noting that the crack opens approximately during the tensile half-cycle. In this case, the compressive

half-cycle does not have an important effect on the crack growth (Faanes and Fernando, 1994; Faanes, 1995; Hills and Nowell, 1994). Note that the maximum K_{I} and K_{II} values are obtained when the crack is totally open, since the tangential slip of crack faces are not hindered by the compressive stresses acting on crack faces (Faanes, 1995; Hills and Nowell, 1994; Dubourg and Lamacq, 2000). Under this assumption we have taken $\Delta K = K_{\max}$.

Both problems are modelled with 4-node bilinear quadrilateral elements. The minimum element size in this zone is $h_{\mathrm{e}} = 10\,\mu$m (see Fig. 1). This element size enables the modelling of small cracks that are still longer than h_{e}. An alternative X-FEM formulation for modelling short cracks when compared to the element size can be found in Bellec and Dolbow (2003). At this point, the question of the suitability of the initial crack length a_0 arises. An initial value of $a_0 = 50\ \mu$m has been assumed. This size is of the order of several grains for this material, a necessary condition for the applicability of the LEFM. The initial crack size has also been estimated using the El Haddad equation (El Haddad et al., 1979):

$$a_0 = \frac{1}{\pi}\left(\frac{\Delta K_{\mathrm{th}}}{\sigma_{N=10^6}}\right)^2. \tag{5}$$

The following values were found in Wittkowsky et al. (2000) for the aluminum alloy 7075-T6: plain fatigue limit (in terms of stress amplitude) $\sigma_{N=10^6} = 214$ MPa and threshold value $\Delta K_{\mathrm{th}} = 2.2\,\mathrm{MPa\,m^{1/2}}$ (both for $R = -1$). Using Eq. (5), the estimation $a_0 = 33.6\,\mu$m is obtained, which is in good agreement with the grain size perpendicular to the surface of $35\,\mu$m reported by Navarro et al. (2003), measured according to ASTM Standards. Therefore the value $a_0 = 50\,\mu$m is considered acceptable.

The friction model assumed for the contact zone is a Coulomb model and

the ABAQUS contact formulation based on Lagrange multipliers is used. The Lagrange multiplier formulation enables the exact modelling of sticking contact conditions, in contrast to contact formulations based on penalty methods (these require a certain amount of slip, the so-called elastic slip dependent on the penalty constant, to develop a sticking frictional shear traction). The exact modelling of sticking conditions is an important issue in fretting problems (Goh et al., 2003), to resolve the stick/slip behaviour along the interface.

5 NUMERICAL RESULTS AND DISCUSSION

5.1 Problem 1: Complete contact problem

In Fig. 5, an enlarged detail of the deformed shape (σ_{xx} stress field) of the extended finite element model analyzed with ABAQUS is illustrated. The deformation due to the implicit crack opening can be observed at the instant of maximum amplitude $\sigma_{\mathrm{B,max}}$. As explained earlier, this opening is generated by the mathematical discontinuity present in the enriched elements. The steep stress gradient in the vicinity of the crack tip can be seen. Note also the expected σ_{xx} stress discontinuity across the indenter interface due to the sliding contact conditions. User defined elements (enriched elements in this application) are marked with crosses by ABAQUS, indicating the position of the first node in the connectivity of the enriched element. Of course, the first node in the connectivity is not necessarily an enriched node.

The crack propagation path for each of the cases considered for $\sigma_{\mathrm{B,max}}$ is shown in Fig. 6. The number of crack increments is 20, with value $\Delta a = a_0 = 50\,\mu$m. The radius of the q-function (Moës et al., 1999) used in the domain interaction

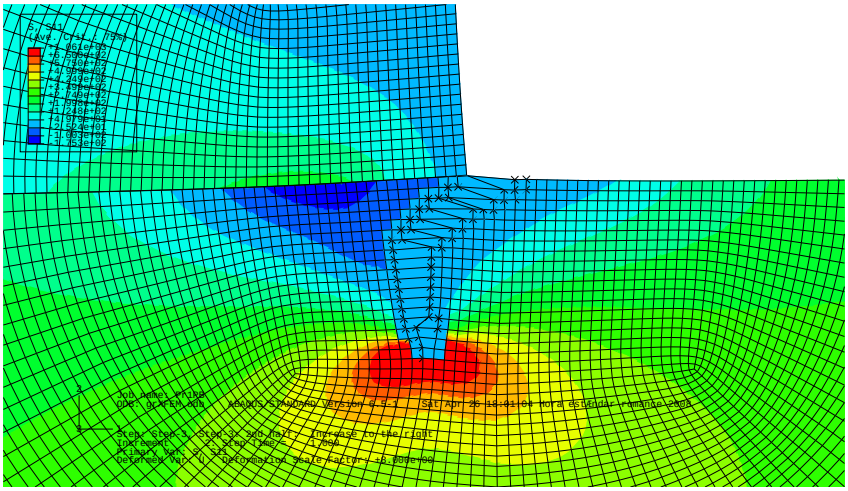

Fig. 5. Enlarged view of the deformed shape for the σ_{xx} stress field at the instant when $\sigma_{\mathrm{B}}(t)$ is maximum. Scale factor: 8x.

integral has been taken as $r_q = 40\mu$m (the minimum element size in this zone is $h_{\mathrm{e}} = 10\,\mu$m). Like the initial length a_0, the initial crack orientation $\theta_{c,0}$ must also be defined. In principle, this value can be inferred from experimental information found in the literature (Adibnazari and Hoeppner, 1994; Mutoh et al., 2003). The application of certain critical plane methods to estimate the angle of initiating cracks could also be used (Lamacq et al., 1997). For all cases of Fig. 6, the initial angle $\theta_{c,0}$ is 60$^{\mathrm{o}}$ with respect to the free surface of the specimen. For larger values of $\sigma_{\mathrm{B,max}}$, it can be observed that the influence of the contact zone due to σ_{P} is less significant and the crack tends to grow in a direction normal to the bulk load σ_{B}.

For low bulk loads $\sigma_{\mathrm{B,max}}$, it can be noticed that there is an abrupt change of direction departing from the initial crack angle $\theta_{c,0} = 60^{\mathrm{o}}$. Hence, it is indicative that the true initial angle for those load conditions is different from the one assumed *a priori*. The effect of the assumed initial crack angle $\theta_{c,0}$ is studied in Fig. 7. The results reveal that the value of $\theta_{c,0}$ does not strongly affect the orientation after a few crack increments, because the crack propagation

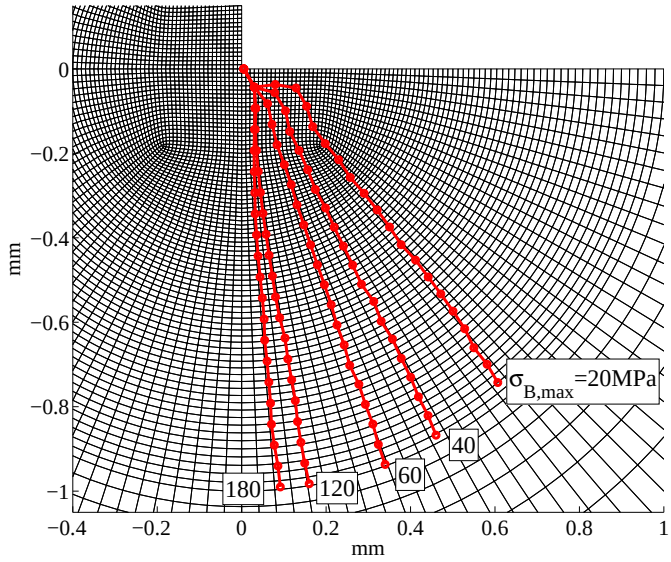

Fig. 6. Crack propagation paths for several values of $\sigma_{\mathrm{B,max}}$. The initial crack angle is $\theta_{c,0} = 60^{\mathrm{o}}$.

follows a natural path based on the maximum energy that is released. For low values of $\sigma_{\mathrm{B,max}}$, the calculated SIFs are very low for the first crack increments (in some cases, even less than the threshold value used in long crack growth models, like Paris's law). This issue has not been considered in this study and it has been assumed that the crack eventually propagates in all cases.

Fig. 8 proves that a refined discretization of the crack increment (20 increments with $\Delta a = 25\ \mu$m instead of $\Delta a = 50\ \mu$m) leads basically to the same results shown in Fig. 6. The agreement revealed in Fig. 8 demonstrates the robustness of the X-FEM: for $\Delta a = 25\ \mu$m, the radius of the q-function r_q is $24\ \mu$m, which implies that very few elements are contributing to the domain integral computation because $h_{\mathrm{e}} = 10\ \mu$m in this zone. However, the quality of the estimation is still good.

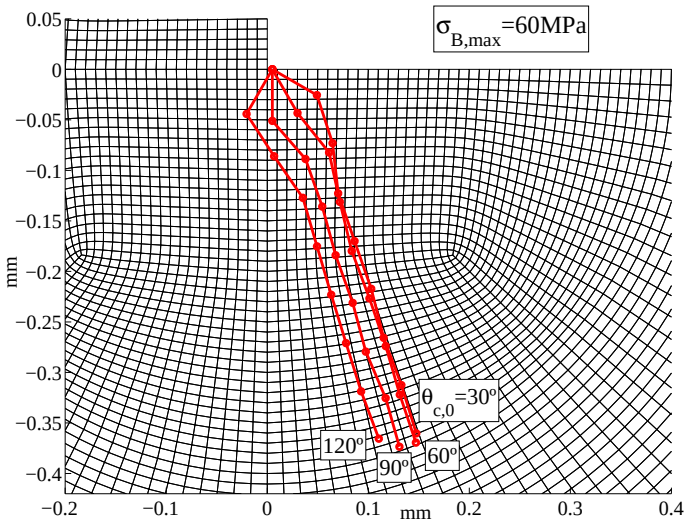

Fig. 7. Effect of the initial crack angle $\theta_{c,0}$ on the propagation path. Load case $\sigma_{\mathrm{B,max}} = 60\mathrm{MPa}$.

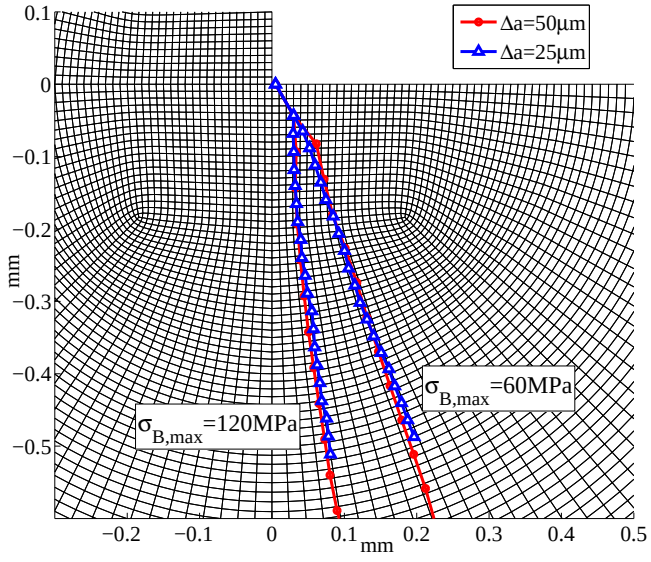

Fig. 8. Effect of the crack increment size $\Delta a = 25\,\mu$m and $50\,\mu$m on the propagation path. The initial crack is the same in both cases.

5.2 SIF calculations for Problem 1 (complete contact problem)

In order to estimate the orientation angle θ_c using Eq. (4), all previous analyses need the computation of K_{I} and K_{II} for each crack growth increment. Since

the SIF extraction with the interaction integral is based on the numerical solution provided by the X-FEM, it is convenient to assess the quality of the SIF computation, which is obviously affected by the discretization error (like in a standard FE formulation). In this subsection, we compare some SIFs calculations using the presented approach with other analytical solutions of reference for certain configurations.

Fig. 9 shows the value of K_{I} vs. the crack length a for a crack located at the end of the contact zone. In order to make feasible the comparison with reference solutions, the crack is enforced to be normal to the contact surface (i.e. no crack deviation is allowed). One of the plotted series of results has been calculated with only bulk load on the specimen and no contact pressure on the indenters. The corresponding SIFs agree very well with the analytical approximation given in Tada et al. (1985) for a double edge crack in a strip of finite width in tension (DENT). As expected, the approximation with a single edge crack solution (SENT) is only valid for short cracks (less than 7% of the half thickness of the specimen w). The SIF solution for the fretting fatigue loading condition (bulk load combined with the normal load on the indenter) is also plotted in Fig. 9. The effect of the contact load is to increase the severity of the crack, yielding larger values of K_{I} than for a plain fatigue situation. This effect agrees well with the experimental evidence reported in the literature (see for example Hills and Nowell, 1994), as fretting tends to induce faster crack growth rates than plain fatigue during the early propagation stages. As the crack grows, the contact influence decreases and the behaviour approaches that of plain fatigue.

This latter series of fretting fatigue results has been also estimated in this work using weight functions, an analytical procedure that, together with the

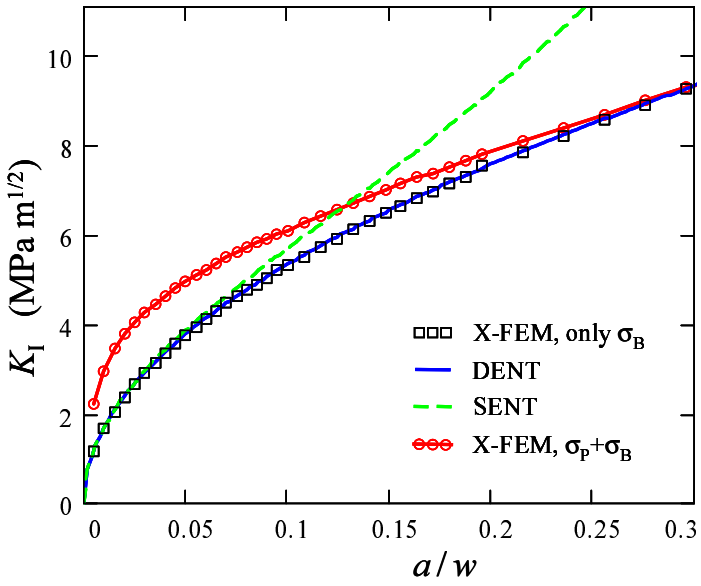

Fig. 9. Problem 1: Mode I SIF vs. crack length a for a series of cracks located at the end of the contact zone, which are all normal to the contact surface.

Green's function technique, is often used in the fracture mechanics approach to fretting fatigue (Faanes and Fernando, 1994; Navarro et al., 2003). Analytical approaches in literature make use of the knowledge of the theoretical contact stress fields to estimate the SIFs. In the weight function formulation (Bueckner, 1973) the stress distribution along the crack location (solved for a configuration without a crack) is combined with a weight function $w(y)$ derived for a given geometry to yield K:

$$K_{\mathrm{I}}^{\mathrm{WF}} = \sqrt{\frac{2}{\pi}} \int_0^a \sigma_x(x,y) w(y)\, \mathrm{d}y. \tag{6}$$

In the case considered here of a straight crack normal to the surface at the end of the contact zone ($x = 0$, see Fig. 3), the stresses σ_x for a no-crack configuration must be known along the y-direction (the direction of the normal crack). However, there is no analytical solution available for the finite domain geometry of Problem 1, so we have calculated the generalized stress intensity factors (GSIF) that characterize the singular field in the vicinity of the corner

of a complete contact. In this way, we can have a description of the singular contact field for the given loads and geometry.

With no crack, the bulk stress provokes a relative slip with friction of the contact zone next to the corner. However, the presence of a crack next to the contact zone tends to preclude the partial slip, since the discontinuity of the crack diverts the path followed by the bulk forces. The contact pressure is very high in this zone (it is theoretically singular at the corner) and the shear traction needed to cause partial slip can not be reached when the bulk forces are diverted due to the crack discontinuity. Therefore, it is reasonable to assume that the contact zone sticks when a crack is present in the analyzed model. This has been confirmed numerically. For a totally adhered contact zone, the singular field adjacent to the corner can be thought of as forming a V-notch problem. The singular field derived by Williams for a re-entrant or V-notch corner is (Williams, 1952):

$$\left\{ \begin{array}{c} \sigma_{rr}(r,\theta) \\ \\ \sigma_{\theta\theta}(r,\theta) \\ \\ \sigma_{r\theta}(r,\theta) \end{array} \right\} = K_{\mathrm{I}}^{\mathrm{GSIF}}\ r^{\lambda_{\mathrm{I}}-1}\ \boldsymbol{\Psi}^{\mathrm{I}}(\theta) + K_{\mathrm{II}}^{\mathrm{GSIF}}\ r^{\lambda_{\mathrm{II}}-1}\ \boldsymbol{\Psi}^{\mathrm{II}}(\theta) \qquad (7)$$

where the trigonometric functions $\boldsymbol{\Psi}^{\mathrm{I}}(\theta)$, $\boldsymbol{\Psi}^{\mathrm{II}}(\theta)$ are defined in Appendix A. The eigenvalues in our problem are $\lambda_{\mathrm{I}} = 0.5445$, $\lambda_{\mathrm{II}} = 0.9085$ (see Appendix A). The values of $K_{\mathrm{I}}^{\mathrm{GSIF}}$ and $K_{\mathrm{II}}^{\mathrm{GSIF}}$ were estimated using stress extrapolation from the FE solution for a no-crack configuration, yielding 26.21 $\mathrm{MPa\,mm}^{1-\lambda}$ and -177.75 $\mathrm{MPa\,mm}^{1-\lambda}$, respectively. In this way, the singular field due to the contact corner can be reconstructed via (7) and used as an approximation to $\sigma_x(x,y)$ in (6). Fig. 10 shows the estimation of K_{I} computed

using (6). It can be seen that the agreement with the extended finite element solution is good for very small cracks, where the singular field dominates. Due to the small crack size, this agreement is attained with both the single-edge crack weight function (SENT) given by Bueckner (1973) and with the more appropriate double-edge crack weight function (DENT) given by Fett et al. (1988). Obviously, the solution for a DENT weight function tends to approach the extended finite element solution for longer cracks.

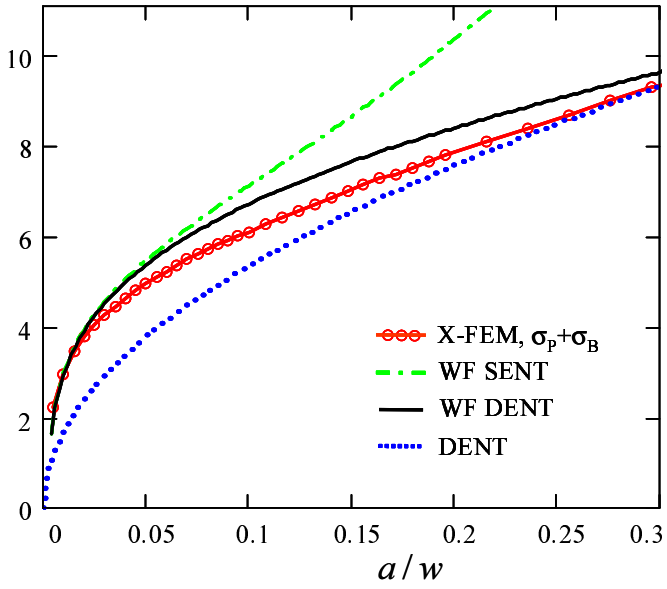

Fig. 10. Problem 1: Mode I SIF vs. crack length a for a series of cracks located at the end of the contact zone, which are all normal to the contact surface. Comparison with analytical computations using weight functions.

From the above analysis for normal cracks, we conclude that the X-FEM yields good estimations of the SIF. We must point out that the extended finite element method is not restricted to normal straight cracks, but allows the analysis of more complex crack geometries, including inclined and kinked geometries. In addition, since the X-FEM inherits the main advantages of the FEM, the influence of nearby boundaries is also considered, which can be more

involved in other methods, such as the distributed dislocation technique (Hills and Nowell, 1994).

Finally, in Fig. 11 we represent the numerical value of K_{I} and K_{II} as well as the orientation angle calculated with Eq. (4) vs. crack length (measured as the addition of the crack growth increments) for the case $\sigma_{\mathrm{B,max}} = 120$MPa shown in Fig. 6. It can be observed that the propagation path tends to minimize the value of K_{II} and that the sign of K_{II} is opposite to the θ_c sign, according to the customary sign convention. As expected, the values of K_{I} increase with the crack length and can be identified with ΔK_{I}.

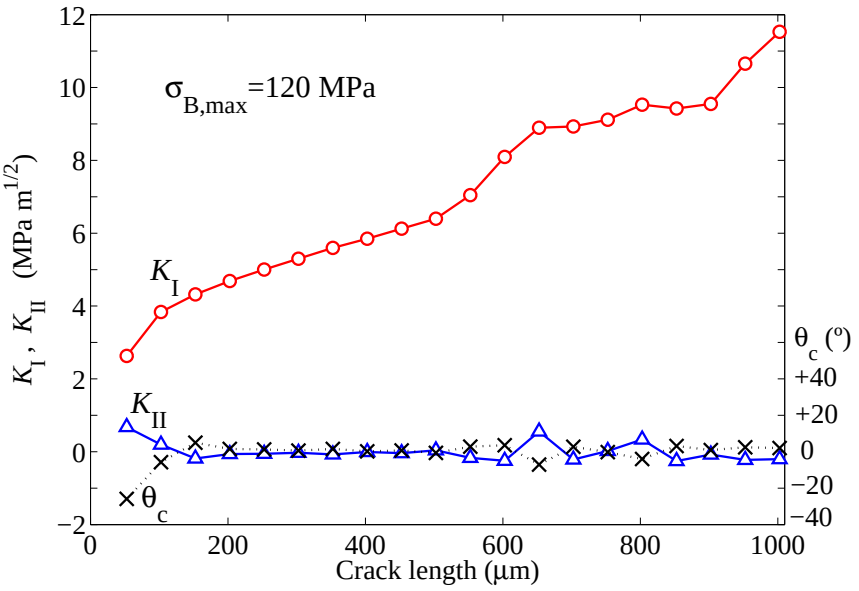

Fig. 11. Problem 1: SIFs values and orientation angle for the case $\sigma_{\mathrm{B,max}} = 120$MPa shown in Fig. 6.

5.3 Problem 2: Incomplete contact problem

The approach presented in this study can be applied to other geometries and contact conditions. We introduce now the incomplete contact problem to show

the good behaviour of the implementation under conditions of partial slip. Unlike in complete contacts, the contact pressure distribution is Hertzian, decreasing rapidly near the end of the contact zone, and a partial slip zone is developed (Hills and Nowell, 1994). Fig. 12 shows the variation of the partial slip zones along the contact width $2a_{\mathrm{H}}$ for a no-crack case and for two different crack lengths. The presence of a normal crack of length $a = 0.17a_{\mathrm{H}}$ located at the end of the contact ($x = a_{\mathrm{H}}$) reduces the amount of partial slip near the crack, due to the stress redistribution and the 'shading' effect of the crack. For a longer crack $a = 1.12a_{\mathrm{H}}$, this effect leads to complete sticking at the left hand side of the crack ($x < a_{\mathrm{H}}$). Note also that some nodes located at the right hand side of the crack ($x > a_{\mathrm{H}}$) enter into contact due to the stress redistribution and experience a large relative slip caused by the traction of the bulk stress. This analysis shows that the X-FEM implementation carried out in this work is capable of representing stick-slip transitions along the contact zone.

In Fig. 13 we represent an estimation of the crack growth path during the propagation stage for the incomplete contact problem. The analysis has been carried out for the loading conditions described in Section 4. An initial crack of 40 μm with an angle $\theta_{c,0} = 120^{\mathrm{o}}$ located at the end of the contact zone has been assumed. The crack path agrees very well with the results presented by Hills and Nowell (1994) for similar loading conditions and where the crack trajectory is computed as the orthogonal direction to the maximum positive principal stress.

The proposed methodology can be very useful for the estimation of the propagation life in fretting fatigue problems due to the positive attributes of the method, namely its robustness, accuracy, ease of geometric modelling of the

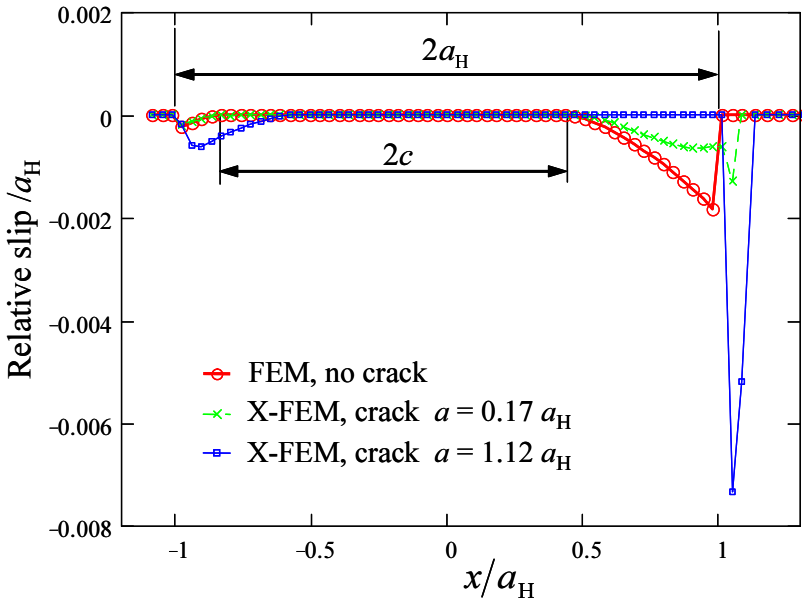

Fig. 12. Problem 2: Variation of the partial slip zone due to the crack presence at the end of the contact zone $x = a_H$. Effect of different crack lengths.

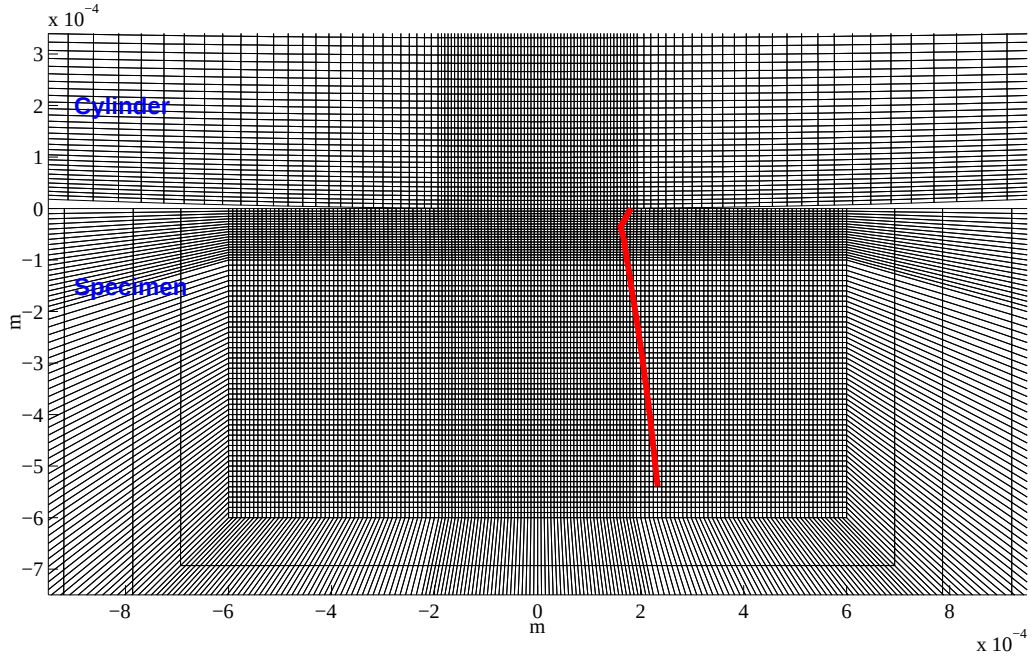

Fig. 13. Problem 2: Estimation of crack growth during the propagation stage.

crack and the inclusion of the contact model with friction. The estimation of the propagation life in fretting is considered in the literature (Faanes and Fernando, 1994; Faanes, 1995; Mutoh et al., 2003) based on the SIFs calculated under contact influence. Navarro et al. (2003) compute the SIF using weight functions during the propagating stage. In general, these studies are based on simplifications regarding the crack shape and the effects of contact tractions. Following the approach we have pursued, such simplifications in the numerical model are circumvented, and more accurate SIFs are realized. This is especially important when using crack growth laws for estimating propagation lives that strongly depend on the accuracy of the SIFs.

There are other important issues that have not been addressed in this work, which deserve further attention, such as the study over complete cycles including crack closure effects. To study crack closure effects, X-FEM formulations that include frictional contact between crack faces (Dolbow et al., 2001; Kim et al., 2007; Ribeaucourt et al., 2007) are promising.

6 CONCLUSIONS

The combination of the advantages of the X-FEM and the inherent capabilities in ABAQUS for modelling contact problems has lead to a methodology for the analysis of crack propagation in fretting fatigue problems. The X-FEM has been implemented in the commercial code ABAQUS by means of user-element subroutines. The use of X-FEM in fretting fatigue introduces a number of distinct benefits over existing models that appear in the literature. The main advantage is that modelling any crack location and orientation becomes a straightforward task, using an easily generated single mesh. This

allows the simulation of crack propagation in a computationally elegant, simple, and cost-effective manner. In addition, the methodology provides accurate SIF extractions through energetic methods based on domain integrals. The accuracy attained is much better than with a standard FE formulation due to the use of crack-tip enrichment functions that adapt much better than the FE solution to the singular crack-tip fields.

In this paper, the methodology has been applied to complete and incomplete contact problems. The influence of the bulk load, the effect of the initial crack angle $\theta_{c,0}$ and the crack increment Δa have been studied, as well as the performance of the implementation under sticking or partial slip conditions. The proposed methodology is robust and accurate and allows the study of several crack configurations. The numerical results demonstrate the merits of the X-FEM for the estimation of the fretting fatigue life during the propagation stage.

Acknowledgements

The authors wish to thank Ministerio de Ciencia y Tecnología for the support received in the framework of the project DPI2007-66995-C03-02. The financial support received from Vicerrectorado de Investigación, Desarrollo e Innovación (Universidad Politécnica de Valencia) and Conselleria d'Empresa, Universitat i Ciència (Generalitat Valenciana) through the project GV06/124 is also gratefully acknowledged. This support enabled the research visit of E. Giner to UC Davis, where parts of this research were accomplished.

A The V-notch solution

In accordance with the polar reference system of Fig. A.1, the stress field can be decomposed into two parts: a symmetric solution with respect to $\theta = 0$ (i.e. the bisector line BB) and an antisymmetric solution (Williams, 1952). The trigonometric functions $\mathbf{\Psi}^{\mathrm{I}}(\theta)$, $\mathbf{\Psi}^{\mathrm{II}}(\theta)$ that define the singular stress field given in (7) have the following components:

$$\mathbf{\Psi}^{\mathrm{I}}(\theta) = \lambda_{\mathrm{I}}(\lambda_{\mathrm{I}}+1)\left\{\begin{array}{l} \cos(\lambda_{\mathrm{I}}+1)\theta\,\dfrac{\cos(\lambda_{\mathrm{I}}-1)\alpha}{\cos(\lambda_{\mathrm{I}}+1)\alpha} - \dfrac{\lambda_{\mathrm{I}}-3}{\lambda_{\mathrm{I}}+1}\cos(\lambda_{\mathrm{I}}-1)\theta \\ -\cos(\lambda_{\mathrm{I}}+1)\theta\,\dfrac{\cos(\lambda_{\mathrm{I}}-1)\alpha}{\cos(\lambda_{\mathrm{I}}+1)\alpha} + \cos(\lambda_{\mathrm{I}}-1)\theta \\ -\sin(\lambda_{\mathrm{I}}+1)\theta\,\dfrac{\cos(\lambda_{\mathrm{I}}-1)\alpha}{\cos(\lambda_{\mathrm{I}}+1)\alpha} + \dfrac{\lambda_{\mathrm{I}}-1}{\lambda_{\mathrm{I}}+1}\sin(\lambda_{\mathrm{I}}-1)\theta \end{array}\right\} \tag{A.1}$$

$$\mathbf{\Psi}^{\mathrm{II}}(\theta) = \lambda_{\mathrm{II}}(\lambda_{\mathrm{II}}+1)\left\{\begin{array}{l} \sin(\lambda_{\mathrm{II}}+1)\theta\,\dfrac{\sin(\lambda_{\mathrm{II}}-1)\alpha}{\sin(\lambda_{\mathrm{II}}+1)\alpha} - \dfrac{\lambda_{\mathrm{II}}-3}{\lambda_{\mathrm{II}}+1}\sin(\lambda_{\mathrm{II}}-1)\theta \\ -\sin(\lambda_{\mathrm{II}}+1)\theta\,\dfrac{\sin(\lambda_{\mathrm{II}}-1)\alpha}{\sin(\lambda_{\mathrm{II}}+1)\alpha} + \sin(\lambda_{\mathrm{II}}-1)\theta \\ \cos(\lambda_{\mathrm{II}}+1)\theta\,\dfrac{\sin(\lambda_{\mathrm{II}}-1)\alpha}{\sin(\lambda_{\mathrm{II}}+1)\alpha} - \dfrac{\lambda_{\mathrm{II}}-1}{\lambda_{\mathrm{II}}+1}\cos(\lambda_{\mathrm{II}}-1)\theta \end{array}\right\}. \tag{A.2}$$

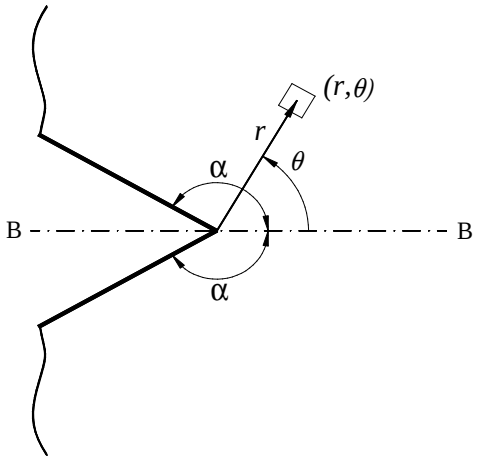

Fig. A.1. V-notch in an infinite half-space.

In (7) the eigenvalue λ_{I} is the lowest positive solution of the so-called characteristic equation for the symmetric solution:

$$\lambda_{\mathrm{I}} \sin(2\alpha) + \sin(2\lambda_{\mathrm{I}}\alpha) = 0 \tag{A.3}$$

and corresponds to the most singular solution. Analogously, the eigenvalue λ_{II} is the lowest positive solution of the characteristic equation for the antisymmetric solution:

$$\lambda_{\mathrm{II}} \sin(2\alpha) - \sin(2\lambda_{\mathrm{II}}\alpha) = 0. \tag{A.4}$$

References

Adibnazari, S., Hoeppner, D.W., 1994. The role of normal pressure in modelling fretting fatigue. ESIS 18. In: Fretting Fatigue (Edited by R.B. Waterhouse and T.C. Lindley). Mechanical Engineering Publications Ltd, London, pp. 125–133.

Anderson, T.L., 1995. Fracture Mechanics: Fundamentals and Applications. 2nd Ed. CRC Press, Boca Raton.

Bellec, J., Dolbow, J.E., 2003. A note on enrichment functions for modelling crack nucleation. Communications in Numerical Methods in Engineering 19, 921–932.

Bueckner, H.F., 1973. Field singularities and related integral representations. In: Mechanics of Fracture 1. Methods of analysis and solutions of crack problems, ed. G.C. Sih. Noordhoff International Publishing, Leyden, pp. 239–314.

Chen, F.H.K., Shield, R.T., 1977. Conservation laws in elasticity of the J-integral type. Journal of Applied Mathematics and Physics (ZAMP) 28, 1–22.

Dai, D.N., Hills, D.A., Nowell, D., 1994. Stress intensity factors for three-dimensional fretting fatigue cracks. ESIS 18. In: Fretting Fatigue (Edited by R.B. Waterhouse and T.C. Lindley). Mechanical Engineering Publications Ltd, London, pp. 59–71.

Dolbow, J., Moës, N., Belytschko, T., 2001. An extended finite element method for modeling crack growth with frictional contact. Computer Methods in Applied Mechanics and Engineering 190 (51-52), 6825–6846.

Dubourg, M.C., Lamacq, V., 2000. Stage II crack propagation direction determination under fretting fatigue loading: a new approach in accordance with experimental observations. In: Fretting Fatigue: Current Technology and Practices. Edited by D.W. Hoeppner, V. Chandrasekaran and C.B. Elliot). ASTM STP 1367, West Conshohocken, pp. 436–450.

El Haddad, M.H., Topper, T.H., Smith, K.N., 1979. Prediction of non propagating cracks. Engineering Fracture Mechanics 11 (3), 573–584.

Erdogan, F., Sih, G.C., 1963. On the crack extension in plates under plane loading and transverse shear. Journal of Basic Engineering 85, 519-527.

Faanes, S., 1995. Inclined cracks in fretting fatigue. Engineering Fracture Mechanics 52 (1), 71–82.

Faanes, S., Fernando, U.S., 1994. Influence of contact loading on fretting fatigue behaviour. Fatigue and Fracture of Engineering Matererials and Structures 17 (8), 939–947.

Faanes, S., Härkegård, G., 1994. Simplified stress intensity factors in fretting fatigue. ESIS 18. In: Fretting Fatigue (Edited by R.B. Waterhouse and T.C. Lindley). Mechanical Engineering Publications Ltd, pp. London, 73–81.

Fett, T., Stamm, H., Walz, G., 1988. Weight function for finite strip with double-edge notches. Theoretical and Applied Fracture Mechanics 10, 227–230.

Goh, C.H., Neu, R.W., McDowell, D.L., 2003. Influence of nonhomegeneous material in fretting fatigue. In: Fretting Fatigue: Advances in Basic Understanding and Applications (Edited by S.E. Kinyon, D.W. Hoeppner and Y. Mutoh). ASTM STP 1425, West Conshohocken, pp. 183–205.

Hattori, T., Nakamura, M., Watanabe, T., 2003. Simulation of fretting fatigue life by using stress-singularity parameters and fracture mechanics. Tribology International 36, 87–97.

Hibbitt, Karlsson & Sorensen, Inc., 2004. ABAQUS/Standard User's Manual, V. 6.5, Pawtucket, Rhode Island.

Hills, D.A., Nowell, D., 1994. Mechanics of fretting fatigue. Kluwer Academic Publishers, Dordrecht.

Huang, R., Sukumar, N., Prévost, J.-H., 2003. Modeling quasi-static crack growth with the extended finite element method. Part II: Numerical applications. International Journal of Solids and Structures 40 (26), 7539–7552.

Kim, T.Y., Dolbow, J., Laursen, T., 2007. A mortared finite element method for frictional contact on arbitrary interfaces. Computational Mechanics 39, 223–235.

Kimura, T., Sato, K., 2003. Simplified method to determine contact stress distribution and stress intensity factors in fretting fatigue. International Journal of Fatigue 25, 633–640.

Lamacq, V., Dubourg, M.C., Vincent, L., 1996. Crack path prediction under fretting fatigue. A theoretical and experimental approach. Journal of Tribology 118, 711–720.

Lamacq, V., Dubourg, M.C., Vincent, L., 1997. A theoretical model for the prediction of initial growth angles and sites of fretting fatigue cracks. Tribology International 30 (6), 391–400.

Moës, N., Dolbow, J., Belytschko, T., 1999. A finite element method for crack

growth without remeshing. International Journal for Numerical Methods in Engineering 46 (1), 131–150.

Mutoh, Y., Xu, J.Q., Kondoh, K., 2003. Observations and analysis of fretting fatigue crack initiation and propagation. In: Fretting Fatigue: Advances in Basic Understanding and Applications (Edited by S.E. Kinyon, D.W. Hoeppner and Y. Mutoh). ASTM STP 1425, West Conshohocken, pp. 61–75.

Navarro, C., García, M., Domínguez, J., 2003. A procedure for estimating the total life in fretting fatigue. Fatigue and Fracture of Engineering Matererials and Structures 26 (5), 459–468.

Ribeaucourt, R., Baietto-Dubourg, M.-C., Gravouil, A., 2007. A new fatigue frictional contact crack propagation model with the coupled X-FEM/LATIN method. Computer Methods in Applied Mechanics and Engineering 196, 3230-3247.

Richard, H.A., Fulland, M., Sander, M., 2005. Theoretical crack path prediction. Fatigue and Fracture of Engineering Matererials and Structures 28, 3-12.

Rubinstein, A.A., 1991. Mechanics of the crack path formation. International Journal of Fracture 47, 291–305.

Sheikh, M.A., Fernando, U.S., Brown, M.W., Miller, K.J.M., 1994. Elastic stress intensity factors for fretting cracks using the finite element method. ESIS 18. In: Fretting Fatigue (Edited by R.B. Waterhouse and T.C. Lindley). Mechanical Engineering Publications Ltd, London, pp. 83–101.

Sukumar, N., Prévost, J.-H., 2003. Modeling quasi-static crack growth with the extended finite element method. Part I: Computer implementation. International Journal of Solids and Structures 40 (26), 7513–7537.

Sumi, Y., 1985. Computational crack path prediction. Theoretical and Applied

Fracture Mechanics 4, 149–156.

Tada, H., Paris, P.C., Irwin, G.C., eds., 1985. The stress analysis of cracks handbook. 2nd. ed. Paris Productions, Inc. St. Louis, Missouri.

Ventura, G., Budyn, E., Belytschko, T., 2003. Vector level sets for description of propagating cracks in finite elements. International Journal for Numerical Methods in Engineering 58, 1571–1592.

Williams, M.L., 1952. Stress singularities resulting from various boundary conditions in angular corners of plates in extension. Journal of Applied Mechanics 19, 526–528.

Wittkowsky, B.U., Birch, P.R., Domínguez, J., Suresh, S., 2000. An experimental investigation of fretting fatigue with spherical contact in 7075-T6 aluminum alloy. In: Fretting Fatigue: Current Technology and Practices. Edited by D.W. Hoeppner, V. Chandrasekaran and C.B. Elliot). ASTM STP 1367, West Conshohocken, pp. 213–227.

Yau, J.F., Wang, S.S., Corten, H.T., 1980. A mixed-mode crack analysis of isotropic solids using conservation laws of elasticity. Journal of Applied Mechanics 47, 335–341.

Zi, G., Belytschko, T., 2003. New crack-tip elements for XFEM and applications to cohesive cracks. International Journal for Numerical Methods in Engineering 57, 2221–2240.

FIGURE CAPTIONS

Fig. 1. Enriched nodes in the X-FEM. Circles: nodes with 2 additional dof. Squares: nodes with 8 additional dof.

Fig. 2. Mode I SIF associated with an infinitesimal kinked crack emanating from an existing crack. Non-proportional evolution under varying bulk load for Problem 1.

Fig. 3. Problem 1: complete contact model with flat indenters.

Fig. 4. Problem 2: incomplete contact model with cylindrical pads.

Fig. 5. Enlarged view of the deformed shape for the σ_{xx} stress field at the instant when $\sigma_{\mathrm{B}}(t)$ is maximum. Scale factor: 8x.

Fig. 6. Crack propagation paths for several values of $\sigma_{\mathrm{B,max}}$. The initial crack angle is $\theta_{c,0} = 60^{\mathrm{o}}$.

Fig. 7. Effect of the initial crack angle $\theta_{c,0}$ on the propagation path. Load case $\sigma_{\mathrm{B,max}} = 60\mathrm{MPa}$.

Fig. 8. Effect of the crack increment size $\Delta a = 25\ \mu\mathrm{m}$ and $50\ \mu\mathrm{m}$ on the propagation path. The initial crack is the same in both cases.

Fig. 9. Problem 1: Mode I SIF vs. crack length a for a series of cracks located at the end of the contact zone, which are all normal to the contact surface.

Fig. 10. Problem 1: Mode I SIF vs. crack length a for a series of cracks located at the end of the contact zone, which are all normal to the contact surface. Comparison with analytical computations using weight functions.

Fig. 11. Problem 1: SIFs values and orientation angle for the case $\sigma_{\mathrm{B,max}} = 120\mathrm{MPa}$ shown in Fig. 6.

Fig. 12. Problem 2: Variation of the partial slip zone due to the crack presence at the end of the contact zone $x = a_{\mathrm{H}}$. Effect of different crack lengths.

Fig. 13. Problem 2: Estimation of crack growth during the propagation stage.

Fig A.1. V-notch in an infinite half-space.